Structural Engineering and Mechanics, Vol. 36, No. 3 (2010) 343-361

DOI: http://dx.doi.org/10.12989/sem.2010.36.3.343

A discrete particle model for reinforced concrete fracture analysis

N. Monteiro Azevedo*[1a], J.V. Lemos[1a] and J.R. Almeida[2b]

[1]LNEC, Av. Brasil 101, 1700-066 Lisboa, Portugal
[2]Department of Civil Engineering, Faculdade de Ciências e Tecnologia, UNL, 1700 Monte de Caparica, Portugal

(Received August 20, 2009, Accepted June 27, 2010)

Abstract. The Discrete Element Method adopting particles for the domain discretization has recently been adopted in fracture studies of non-homogeneous continuous media such as concrete and rock. A model is proposed in which the reinforcement is modelled by 1D rigid-spring discrete elements. The rigid bars interact with the rigid circular particles that simulate the concrete through contact interfaces. The DEM enhanced model with reinforcement capabilities is evaluated using three point bending and four point bending tests on reinforced concrete beams without stirrups. Under three point bending, the model is shown to reproduce the expected final crack pattern, the crack propagation and the load displacement diagram. Under four point bending, the model is shown to match the experimental ultimate load, the size effect and the crack propagation and localization.

Keywords: discrete-element; reinforced-concrete; fracture.

1. Introduction

The complex constitutive behaviour of reinforced concrete arising from extensive micro-cracking and macro-cracking is difficult to characterize in terms of a continuum formulation, the presence of steel and its interaction with concrete further increases this difficulty. An appropriate stress-strain law may not exist or the law may be excessively complicated.

Particle models taking directly into consideration the physical mechanisms and the influence of the concrete aggregate-structure have been developed to model fracture in concrete. When compared to continuum formulations, particle methods are conceptually simpler and the creation of cracks and rupture surfaces appear naturally as part of the simulation process given its discrete nature. By simulating the concrete aggregate-structure a particle method prevents the localization of damage into regions not sufficiently large when compared to the inhomogeneity size, Bazant (1986). Within this approach concrete is regarded as a skeleton of aggregate particles of various sizes, almost in direct contact with each other. The cement matrix acts as a filler and adhesive, enabling the

*Corresponding author, Research Officer, Ph.D., E-mail: nazevedo@lnec.pt
[a]Research Officer, Ph.D.
[b]Associate Professor

structure to carry tensile stresses. The parameters in the interaction laws may require some calibration at the micro-level.

The Discrete Element Method DEM was initially introduced for the study of discontinuous rock. Rigid circular particle DEM based models have also been developed for the study of the micro-mechanic behaviour of soils, Cundall and Strack (1979). Circular particle models have also been applied in the study of fracture processes in rock, Potyondy and Cundall (1996), and concrete, Meguro and Hakuno (1989) and Takada and Hassani (1997). This has been accomplished through the development of constitutive models for the inter-particle contacts enabling the transmission of tensile forces through the contact interface. It is important to refer also that lattice type models, which differ from DEM type in the solution procedure and in the model for particle interaction, have also been proposed with success as a micromechanical model to study fracture process in heterogeneous materials, Schlangen and Garboczi (1996).

A 2D rigid circular particle model, based on the DEM, has been recently developed to model concrete fracture, Monteiro Azevedo (2003). This particle model was shown to give a good agreement with concrete experimental data, namely elasticity, fracturing, the peak stress values, the crack initiation and crack localization. All these macroscopic behaviour features are emergent properties of the DEM model that arise given the particle assembly and a relatively simple set of micro-properties. In order to adapt the model to reinforced concrete fracture studies it is further required to consider the reinforcement and the way it interacts with the particle assembly.

In the context of finite element procedures, FEM, three different approaches are usually adopted to represent the reinforcing bars depending on the choice of the problem to be analyzed, see ASCE special publication (1981):

1) Discrete modelling of the reinforcement - One dimensional elements are usually used to represent the reinforcement bars, either truss finite elements with axial deformation or beam elements which allow for axial, shear and bending deformation. The discrete elements representing the steel reinforcement are connected to the concrete through linkage elements with a given spring stiffness. The spring stiffness parallel to the reinforcement usually follows bond-slip laws that can be derived from laboratory results.
2) Distributed modelling of the reinforcement - The reinforcing bars are smeared over the concrete in any specified direction. Perfect bond is assumed which provides displacement compatibility, the element stiffness being defined through a composite constitutive relationship.
3) Embedded modelling of the reinforcement - The reinforcing bar is effectively modelled as an axial member located at its actual position in the concrete finite element. Perfect bond is assumed and the bar displacements are compatible with those of the concrete finite element.

In the context of the DEM based simulations the reinforcement was first modelled as a special contact between two discrete entities, using the same procedure as adopted for the traditional block to block contact, Lorig and Cundall (1987). At each reinforced interface a perfect bond relationship was adopted that was able to describe both the shear and the axial behaviour of the reinforcement element through two springs located at the contact interface and oriented parallel and perpendicular to the steel bar element. For 2D particle circular DEM methods the reinforcement has been modelled in the past, Takada and Hassani (1997) and Morikawa *et al*. (1993), assuming a perfect bond between the concrete and the reinforcement. In the particles intersected by a reinforcement bar two kinds of contacts are taken into consideration, one related with the concrete and the other related with the reinforcement bar. Both contacts are calculated and checked for failure separately using the principles defined for the traditional point contact.

In the context of the rigid body spring method, RBSM, Kawai (1987) which shares some similarities with the DEM, a discrete approach is also followed but adopts a different solution procedure and it imposes less restrictions on the contact modelling, the reinforcement has also been introduced, see Bolander *et al*. (1999) and Saito *et al*. (1999). The reinforcement bars are represented by plane frame finite elements, and given the reinforcement location the generated nodes are located midway along the path traversing each discrete element, which is called cell under the RBSM name convention. The plane frame finite elements degree of freedom are tied into the rigid spring network cell via rigid body arm constraints and zero-size bond link elements in a similar procedure to the one adopted by Ngo *et al*. (1967) which was one of the first attempts to model the reinforcement in the FEM context. Large values of stiffness are associated to the transverse and rotational springs to prevent relative motion between the associated degrees of freedom. The strength and the stiffness of the spring aligned parallel to the reinforcement direction are governed by nonlinear bond-slip relations as determined through experimentation. The effect of bond slip on crack spacing has also been investigated with lattice type models, Chen and Baker (2003), being the reinforcement nodes connected to the interface through a bond-link element.

In a 2D model it is important to adopt a scheme that can capture not only the stiffness contribution over a localized zone of the concrete but also the 3D effect at the interface of the reinforcement bar with the particles that model the concrete. For this reason a procedure using the zero-size bond link elements defined in Ngo *et al*. (1967) is adopted for the interaction between the reinforcement and the intersected discrete particles.

The 2D rigid circular particle model based on the DEM that has been developed to model concrete fracture is briefly described, Monteiro Azevedo (2003). Then, a reinforcement model and a particle/reinforcement interaction model, which have been developed by the authors in order to enable the application of the 2D model to fracture studies of reinforced concrete structures, are presented.

The DEM model proposed model with reinforcement capabilities is evaluated in three point bending, Bosco *et al*. (1990), and in four point bending tests, Bazant and Kazemi (1991), of reinforced concrete beams without stirrups. Under three point bending, the reinforced particle model is shown to predict closely the load displacement relationship. The maximum load values agree well for the several reinforcement areas adopted. The crack propagation and the final crack patterns are also close to the expected behaviour of a reinforced concrete beam. The proposed numerical model is also able to capture the influence of the steel ratio on the response. Under four point bending loading, the particle model is shown to reproduce well the final crack pattern, the crack propagation and the size effect on diagonal shear failure of beams without stirrups.

In recent years 3D meso-particle models have been proposed for the analysis of fracture phenomena in rock and concrete. These models may employ spherical or more complex polyhedrical particles implementing various constitutive assumptions. They are either based on lattice models Lilliu and Van Mier (2003), on discrete element models, Cusatis *et al*. (2003), Potyondi *et al*. (2004), Hentz *et al*. (2004), on the rigid block spring method, Berton and Bolander (2006) or on nonlinear interface finite elements, Caballero *et al*. (2006). Nevertheless, the enhancement of current 2D models should still be carried out. When compared to 3D models, the 2D models can be easily applied in more complex geometries and in larger scales given the fact that the 3D models require a much larger number of particles leading to an extremely high computational cost. For this reason it is faster to test the performance of model enhancements in 2D prior to the development of the equivalent 3D model. The 2D representation of concrete as a circular particle assembly is still an approximation of reality, but it is important to stress out that, as stated previously, its core formulation incorporates important mechanisms such as particle size, particle interaction and random structure. Note that the proposed methodology for the reinforcement model, using rigid bar elements, can be readily extended to 3D.

2. Formulation

2.1 Discrete particles

In the DEM the domain is replaced by an assembly of discrete entities that interact with each other through contact points or contact interfaces. The set of forces acting on each block/particle are related to the relative displacement of the block/particle with respect to its neighbours. Given the applied forces, Newton's 2nd law of motion is applied in order to define the new position of the block/ particle. The relation between the generalized forces transmitted through the contact and applied at the centre of gravity of the particles to the generalized displacements at the centre of gravity of the particles, see Fig. 1, can be expressed by

$$\{f\} = [K^e]\{d\} \tag{1}$$

where, $\{f\}$ is the generalized force vector, $\{d\}$ is the generalized displacement vector and $[K^e]$ is the contact stiffness matrix in terms of particle displacements.

The generalized force and displacement vectors are given, in accordance with Fig. 1, by

$$\{f\} = \{f_1\, f_2\, f_3\, f_4\, f_5\, f_6\}^t, \quad \{d\} = \{d_1\; d_2\; d_3\; d_4\; d_5\; d_6\}^t \tag{2}$$

The single contact element stiffness matrix, $[K^e]$, in terms of particle displacements for a reference plane passing through the normal to the point contact $n_i = (n_1, n_2)$ is defined by

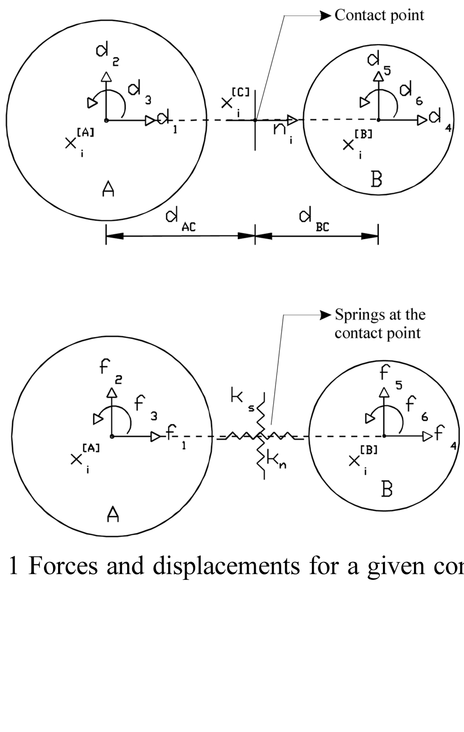

Fig. 1 Forces and displacements for a given contact

$$\begin{bmatrix} k_n & 0 & 0 & -k_n & 0 & 0 \\ 0 & k_s & d_{AC}k_s & 0 & -k_s & d_{BC}k_s \\ 0 & d_{AC}k_s & d_{AC}^2k_s & 0 & -d_{AC}k_s & d_{AC}d_{BC}k_s \\ -k_n & 0 & 0 & k_n & 0 & 0 \\ 0 & -k_s & -d_{AC}k_s & 0 & k_s & -d_{BC}k_s \\ 0 & d_{BC}k_s & d_{AC}d_{BC}k_s & 0 & -d_{BC}k_s & d_{BC}^2k_s \end{bmatrix} \tag{3}$$

where, k_n and k_s are the contact normal and shear stiffness; $d_A = \|x_i^{[A]} - x_I^{[C]}\|$ and $d_B = \|x_i^{[B]} - x_I^{[C]}\|$ are the Euclidean norm of the corresponding vectors; $x_i^{[A]}$ and $x_I^{[B]}$ are the centres of gravity of particles A and B, respectively and $x_I^{[C]}$ represents the contact point coordinates.

An explicit time marching calculation scheme based on the centred-difference algorithm is adopted. At each time step the local stiffness matrix is evaluated and the contact normal direction is updated. The particle forces are then calculated given the inter-particle displacement increments. The total translation stiffness, k_t, and the rotational stiffness, k_θ, of each particle must include, for a given time step, the contribution of all the particles in contact

$$k_t = \sum_{c=1}^{N_c} 2(k_{n,c} + k_{s,c}) \tag{4}$$

$$k_\theta = \sum_{c=1}^{N_c} (d_{BC}^2 k_{s,c} + d_{AC}d_{BC}k_{s,c}) \tag{5}$$

where N_c is the number of particles in contact with the given particle. The contact stiffnesses are defined using

$$k_n = \frac{E'h}{L}t; \quad k_s = \frac{E''h}{L}t \tag{6}$$

where, L is the inter-particle distance, t is the thickness of the particle assembly, h is defined as the contact height, being equal to the smallest diameter of the particles involved, and for plane stress

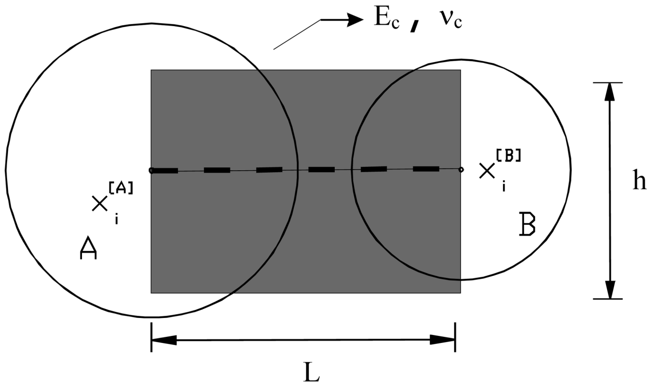

Fig. 2 Schematic representation of interaction stiffness by equivalent elastic continuum volume

$$E' = \frac{E_c}{1 - \nu_c^2} \quad \text{and} \quad E'' = \frac{E_c}{2(1 + \nu_c)} \tag{7}$$

where, E_c and ν_c are the Young's modulus and the Poisson's ratio of the equivalent continuum material. Eq. (6) establishes a simple relationship between macro and micro responses that consider the inter-particle size. The axial and shear spring values are approximated by the axial and shear stiffness of an elastic continuum volume connecting the particles centre of gravity, see Fig. 2.

An explicit time marching calculation scheme based on the centred-difference algorithm is adopted. At each time step, a run is made through all the inter-particle contacts, in order to evaluate the local stiffness matrix, Eq. (3), and the updated contact normal direction. The particle contact forces are then obtained from the inter-particle displacement increments. When only a steady state solution is sought, a density scaling algorithm is adopted in order to reduce the number of time steps necessary to reach the desired solution, Underwood (1983). With this algorithm the particles mass and inertia are artificially scaled so the centred-difference algorithm has a higher rate of convergence for a given loading step. The particle scaled mass and scaled inertia used in the calculations are set given the particle stiffness at a given time increment through

$$m^{scaled} = 0.25k_t; \quad I^{scaled} = 0.25k_\theta \tag{8}$$

In the determination of the contact strength an analogy to the method used in the definition of the contact stiffness is used. The contact strength is set given a simplistic analysis of the equivalent continuum, Fig. 2. The contact strength can then be approximated by

$$F_{n,t\max} = 2.0\sigma_{n,t}R^{\min}t \tag{9}$$

where, $F_{n,t\max}$, is the generalized ultimate contact force, $\sigma_{n,t}$ is the ultimate value of the stress in the desired direction, normal or tangent to the contact plane and $R^{\min}$ is the minimum radius of the particles in contact.

For the inter-particle contacts an extended Mohr-Coulomb model with bilinear softening is adopted, Fig. 3. The bilinear softening diagram is based on the model proposed by Rokugo (1989). Given the adopted fracture energy, representing just the area of the softening part of the diagram, the maximum displacement of a linear softening diagram is defined, U_d^f, Fig. 3. The bilinear diagram is set given the expressions defined in Fig. 3, namely the two points which are required to set a complete a bilinear diagram. When compared to the linear diagram, the bilinear gives a lower resistant force at the beginning of the softening behaviour and allows the particles to interact at a higher distance. The maximum contact strength is directly defined through Eq. (9).

As the calculation progresses the values of the maximum resistant tensile force and maximum cohesion force are reduced as a function of the current value of the contact damage, which is set given the current inter-particle displacement. Contrary to continuum methods, the softening energy is not related to the macroscopic energy of concrete. Fig. 3 also shows that a secant contact stiffness approach is adopted, for this reason the contact stiffness value is also reduced according to the current value of contact damage. In the 2D model, the softening energy is considered to be an indirect way to include effects from the 3rd dimension, and to indirectly account for the effects of the aggregate particle grading, the influence of the particle refinement and the grading of the particles representing the cement paste.

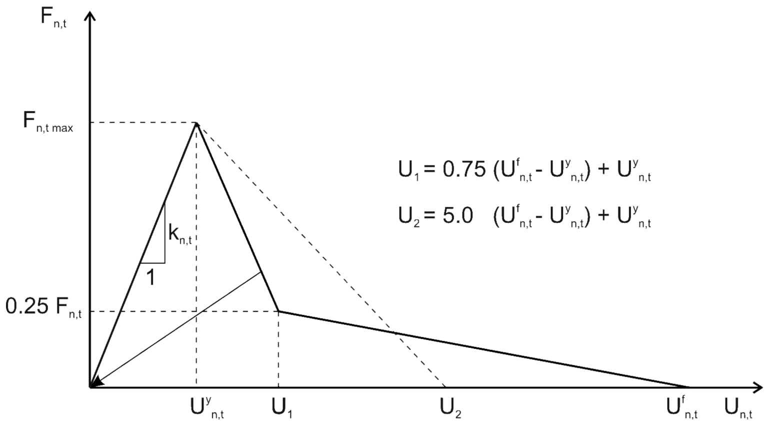

Fig. 3 Contact bilinear constitutive law

At the contact level it is then required to set the ultimate contact tensile stress, σ_t^c, the contact cohesion stress, C^c, the contact friction coefficient, μ^c, the tensile contact fracture energy, G_{ft}^c, and the shear contact fracture energy, G_{ct}^c. Given the contact ultimate stress the corresponding contact strength is defined through Eq. (9).

2.2 Particle generation

The particle configuration is also a model parameter. The modelling of a given structure with the particle method requires the previous definition of the particle distribution based on a given sieve analysis. In Monteiro Azevedo and Lemos (2006) a detailed description of several particle generation algorithms, that allow the generation of compact particles assemblies with the shape, aspect ratio and distribution of the aggregate particles present in concrete, is given. Fig. 4 illustrates for a given aggregate content the adopted approach, first the aggregate particles are inserted from the highest to the smallest diameter without overlapping, followed by the insertion of smaller particles in order to fill the empty space initially surrounding the aggregate particles.

By adopting a particle size and a particle gradation a given dimension is intrinsic to the model which is known to be relevant in concrete, Bazant (1986). The micro-properties are defined adopting a calibration procedure based on a trial and error approach using uniaxial compression and tensile tests data, if available. The elastic values are first set in order to obtain the desired Young's modulus and Poisson's ratio. Then the strength and energy micro-properties are set in order to obtain the desired maximum stress nominal values and tensile fracture energy. The micro-properties

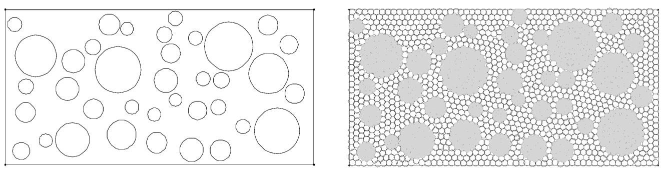

(a) Aggregate (b) Compact assembly

Fig. 4 Particle assemblies – from the aggregate structure to the final compact assembly

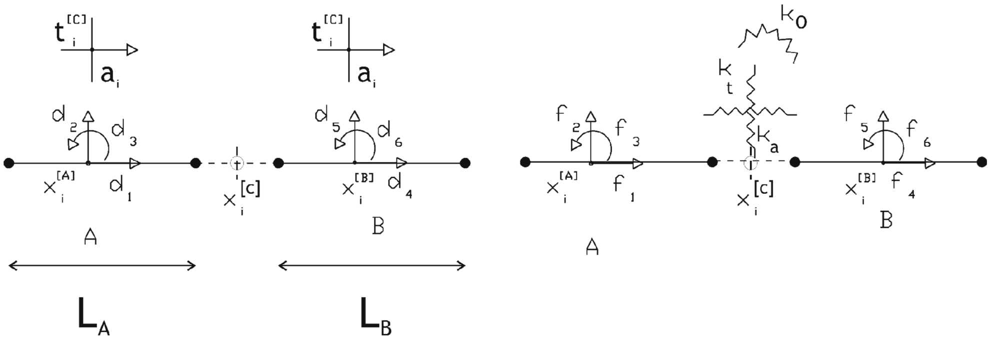

Fig. 5 Forces and displacements for a given reinforcement node

are obviously related with the particle assembly that has been chosen to represent the concrete structure. As computation resources grow, it will be possible to define particle assemblies (aspect ratio, grading and geometry) closer to the concrete structure, and in this way it will be possible to obtain micro-properties closer to reality.

2.3 Proposed reinforcement model

In this work it is proposed to model a given reinforcement through several rigid bar segments that are interacting at the nodal locations. The reinforcement elastic and strength properties are lumped at the rigid bar segment ends. Fig. 5 shows the interaction between two rigid bar segments at the common node. As in the particle model, each rigid bar element has three degrees of freedom of displacement and force at its centre of gravity. Given the contact detection operations that need to be carried with a DEM model, a rigid bar formulation has the advantage that the interaction between the particle and the rigid bar is greatly simplified. With this kind of model, that lumps the elastic and strength properties, it is also easier to set, when compared to traditional linear finite elements, non-linear relationships in the transverse and rotational directions, Kawai (1987).

The nodal rigid bar element stiffness matrix, $[K^e]$, in terms of rigid bars displacements for a reference plane passing through the average to the axial direction $a_i = (a_1, a_2)$ is defined by

$$\begin{bmatrix} k_a & 0 & 0 & -k_a & 0 & 0 \\ 0 & k_t & L_A k_t & 0 & -k_t & L_B k_t \\ 0 & L_A k_t & L_A L_A k_t + k_\theta & 0 & -L_A k_t & L_A L_B k_t - k_\theta \\ -k_a & 0 & 0 & k_a & 0 & 0 \\ 0 & -k_t & -L_A k_t & 0 & k_t & -L_B k_t \\ 0 & L_B k_t & L_A L_B k_t - k_\theta & 0 & -L_B k_t & L_B L_B k_t + k_\theta \end{bmatrix} \tag{10}$$

where, k_a, k_t and k_θ are the axial, transverse and rotational lumped stiffness; L_A and L_B are the lengths of the interacting rigid bars; $x_i^{[A]}$ and $x_I^{[B]}$ are the gravity centres of the rigid bars A and B, respectively. The contact point location, $x_I^{[C]}$, is given by the average nodal location of the nodes that are interacting

$$x_i^{[A]} = 0.5(x_i^{[AJ]} + x_i^{[BI]}) \tag{11}$$

where, $x_i^{[AJ]}$ is the location of the end point of rigid element A, see Fig. 6, and $x_i^{[BI]}$ is the location of the initial point of rigid element B. Both the initial and the end point of each rigid element can be defined at a given time step given the location of the centre of gravity and the current axial direction of the rigid bar. At each time increment the direction of the axial direction of the lumped contact is given by the average of the rigid bar axial directions that are interacting

$$a_i^{[C]} = 0.5(a_i^{[A]} + a_i^{[B]}) \tag{12}$$

The reinforcement nodal lumped stiffnesses are defined using

$$k_a = \frac{EA}{L}; \quad k_t = \frac{12EI}{L^3}; \quad k_\theta = \frac{EI}{L} \tag{13}$$

where, $L = L_A + L_B$ is the total length, A is the reinforcement area and I is the moment of inertia. The total translation stiffness k_t and the rotational stiffness k_θ of each rigid bar element must include, for a given time step, the contribution of all the rigid bar elements in contact

$$K_t = \sum_{r=1}^{N} 2(k_a + k_t) \tag{14}$$

$$K_\theta = \sum_{r=1}^{N} 2(k_\theta + L^2 k_t) \tag{15}$$

where N is the number of rigid bars in contact with the given rigid bar, which in general takes the value of two. Given the maximum values of stiffness, an equivalent procedure to the particle assembly is adopted in order to scale the rigid bar masses. In the numerical results presented an elastic zone followed by a horizontal yield plateau is adopted for the rigid bar element interactions.

2.4 Proposed reinforcement - particle interaction model

In this work an interface model is proposed which allows the interaction between the reinforcement, modelled through discrete rigid linear elements, and the intersected particles,

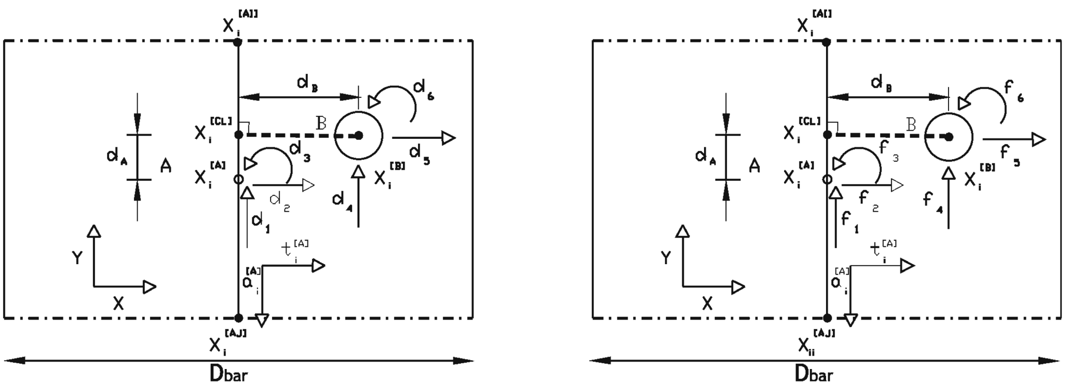

Fig. 6 Forces and displacements for a given reinforcement/particle interface

including the ones over its thickness (bar diameter), Fig. 6. As the bar elements are considered to be rigid, the geometry of each bar is fully defined by the discrete bar length and axial direction.

By adopting a rigid bar element/particle contact interface, the element density used in the reinforcement discretization is made independent of the particle assembly element size. Further, all the particles that intersect a given rigid bar element are considered to interact with it, including the ones that interact over the bar thickness. Only one contact is accepted between a given reinforcement bar modelled through rigid bar elements and a given particle belonging to the particle assembly. Fig. 6 shows the interaction between a particle and a rigid bar element, which enables the modelling of reinforced concrete.

The contact element stiffness matrix, $[K^e]$, that relates rigid bar and particle displacements to rigid bar and particle forces, is defined by

$$\begin{bmatrix} k_a & 0 & 0 & -k_a & 0 & d_B k_a \\ 0 & k_t & -d_A k_t & 0 & -k_t & 0 \\ 0 & -d_A k_t & d_A d_A k_t + k_\theta & 0 & -d_A k_t & -k_\theta \\ -k_a & 0 & 0 & k_a & 0 & -d_B k_a \\ 0 & -k_t & d_A k_t & 0 & k_t & 0 \\ d_B k_a & 0 & -k_\theta & -d_B k_a & 0 & d_B d_B d_a + k_\theta \end{bmatrix} \tag{16}$$

where, k_a, k_t and k_θ are the axial, transverse and rotational interface stiffness; d_A *is* the distance of contact point to the rigid bar centre of gravity; and d_B *is* the distance of contact point to the particle centre of gravity; $x_i^{[A]}$ and $x_I^{[B]}$ are the centres of gravity of rigid bar *A* and particle *B*, respectively. The contact point location, $x_I^{[C]}$, is given by the intersection between the bar axial direction and the bar normal direction starting from the particle centre of gravity, see Fig. 6. The same figure also shows that the interaction between the particle and the steel bar can be at a maximum distance d_B which is bounded by half the thickness of the reinforcement bar.

Given the local stiffness matrix terms, it is also required to add its contribution to the rigid particle and to the rigid bar total translation stiffness k_t and rotational stiffness k_θ. The translation contribution to each element is given by

$$K_t = 2(k_a + k_t) \tag{17}$$

The rotational contributions for the particle and for the rigid bar element are given by

$$K_\theta^{Particle} = 2(k_\theta + k_a d_B^2), \quad K_\theta^{Rigid\ bar} = 2(k_\theta + k_t d_A^2) \tag{18}$$

In the simulations here presented a high value is given to the translational and rotational stiffnesses in order to have a perfect bond on those directions. The yield plateau is defined given the recommended values for confined concrete $\tau = 2.5 f_{ck}^{0.5}$, see CEB-FIP (1990).

For the axial direction a linear elastic zone followed by a yield plateau is adopted for the interface, see Fig. 7. The axial stiffness of the interface is proportional to the rigid bar element lumped stiffness through a "K" multiplier, a value of K = 1 corresponds to an axial stiffness closer to the average inter particle contact stiffness. In the simulations here presented two different values

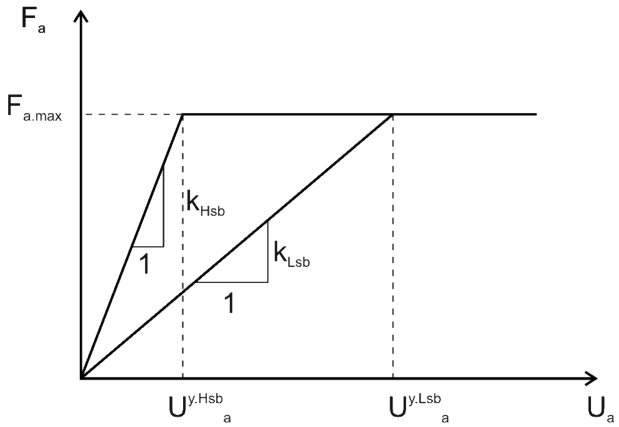

Fig. 7 Bond force-slip relations – higher and lower bond stiffness

of "K" are adopted, a value of K = 0.001 that represents a lower stiffness bond, K_{Lsb}, and a value of K = 5 which represents a higher stiffness bond, K_{Hsb}. A higher stiffness numerically imposes a higher bond between the steel bars and the particles representing the concrete, reducing the slip displacement between the materials. The reduction of the multiplier "K" is an indirect way of numerically reduce the transfer of forces between the two regions. The value de "K" should be calibrated against pull out tests when available. Note that in the simulations here presented the interfaces never reached their maximum axial strength, $F_{a.\max}$, as defined in CEB-FIP (1990). The density of the rigid bar elements was adopted to be closer to a maximum of twice the average diameter of the particulate assembly.

3. Examples

3.1 Three point bending test

The 2D particle model enhanced with the reinforcement and the reinforcement/particle interaction was applied to the analysis of a three point bending test geometry proposed in Bosco *et al*. (1990), which has been used for the analysis of minimum reinforcement in high strength concrete. In Bosco *et al*. (1990) three different size scales were selected, but only the smaller beam is analysed here, see Fig. 8. The concrete, made of crushed aggregate with a maximum size of 12.7 mm, had an

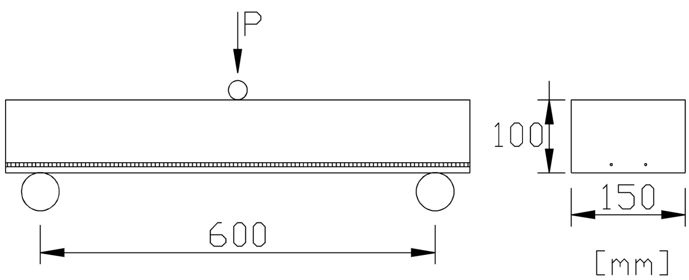

Fig. 8 Three point bending test geometry

Table 1 Elastic and strength properties for the particle model for the three point bending test

E_c [GPa]	ν_c	σ_t^c [MPa]	C^c [MPa]	μ^c [MPa]	G_{ft}^c [N/m]	G_{ct}^c [N/m]
26.8	0.25	5.5	70.0	0.2	16	750

(a) Micro-properties

E [GPa]	ν	G_t [N/m]	σ_t [MPa]	σ_c [MPa]
34.7	0.19	100	5.3	89.6

(b) Macro-properties

average compressive strength of 91.2 MPa, measured in cubic specimens 160 by 160 mm, a fracture energy of 90.0 N/m and a secant Young's modulus of 34.2 GPa.

The micro properties (best-fit values) obtained from a calibration procedure based on compressions tests and tensile tests on 160 by 160 mm cubic particle assemblies are given in Table 1. The calibration procedure is trial/error based. The micro-elastic properties are first calibrated, followed then by the calibration of the strength properties. Table 1 also shows the macroscopic compressive strength, σ_c, macroscopic tensile strength, σ_t, macroscopic tensile fracture energy, G_t, Young's modulus, E, and Poisson's ratio, ν, obtained numerically in the 160 by 160 mm particle assemblies.

In the particle generation procedure an aggregate content of 568.5 kg/m^3 was adopted for particles diameters between 12 mm and 10 mm, and for particle diameters between 8 and 4 mm was considered an aggregate content of 1326.5 kg/m^3. In order to fill the void space around the aggregate structure, a void elimination procedure, see Monteiro Azevedo and Lemos (2006), was carried out by inserting particles with a 4.0 mm diameter. The particle assemblies of the beam tests had an average of 500 aggregate particles and 3500 filling particles.

As in the experiment, several particle assemblies were tested adopting different steel reinforcement areas, see Table 2. The reinforcement was modelled with several discrete rigid segments of 5 mm length. In the numerical tests, the single reinforcement bar had a cross-sectional area equivalent to the total adopted in the experiment. For the steel, a Young's modulus of 200 GPa was assumed. As in the experiment, the distance from the bars to the lower level was set equal to one tenth of the beam depth.

Fig. 9(a) shows one of the particles assemblies tested. Two particles assemblies were tested for each reinforcement case. Fig. 9(b) shows the final displacement of one of the reinforced particle assemblies magnified 20 times. The crack growth evolution is common to the different particles assemblies and to the different steel ratios. Several cracks first appear in the central part underneath the reinforcement close to the maximum bending moment zone. The most central crack would grow

Table 2 Reinforcement properties and corresponding maximum loads

Experiment	Steel content	Yield limit [MPa]	$P_{Experiment}$ [kN]	$P_{Numerical}$ (**K**=0.001) [kN]	$P_{Numerical}$ (**K**=5.0) [kN]
AE 0	0	0	11.8	11.5	-
AE 4	1 Φ 4	637	11.8	11.7	13.7
AE 5	2 Φ 5	569	15.2	13.9	19.7
AE 8	2 Φ 8	441	28.4	27.0	30.3
AE 10	2 Φ 10	456	47.8	43.2	42.8

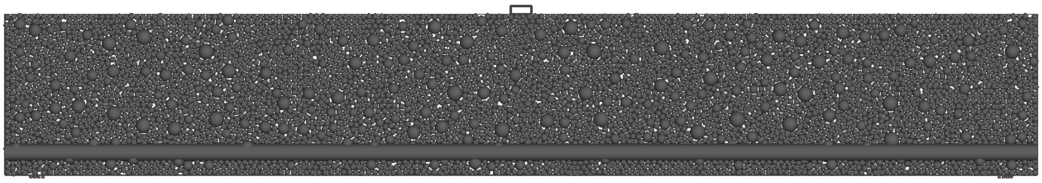

(a) Reinforced particle assembly

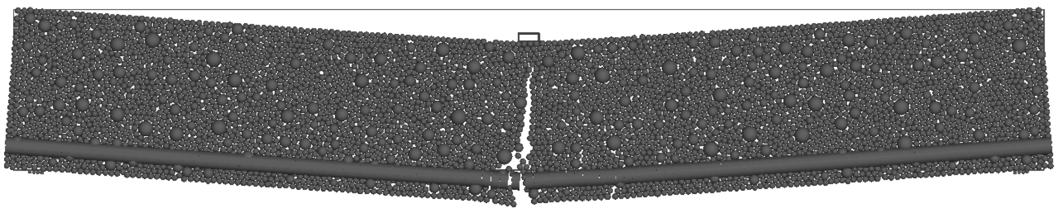

(b) Final displacement (10 times magnified)

Fig. 9 Three point bending test – AE8 (2Φ8)

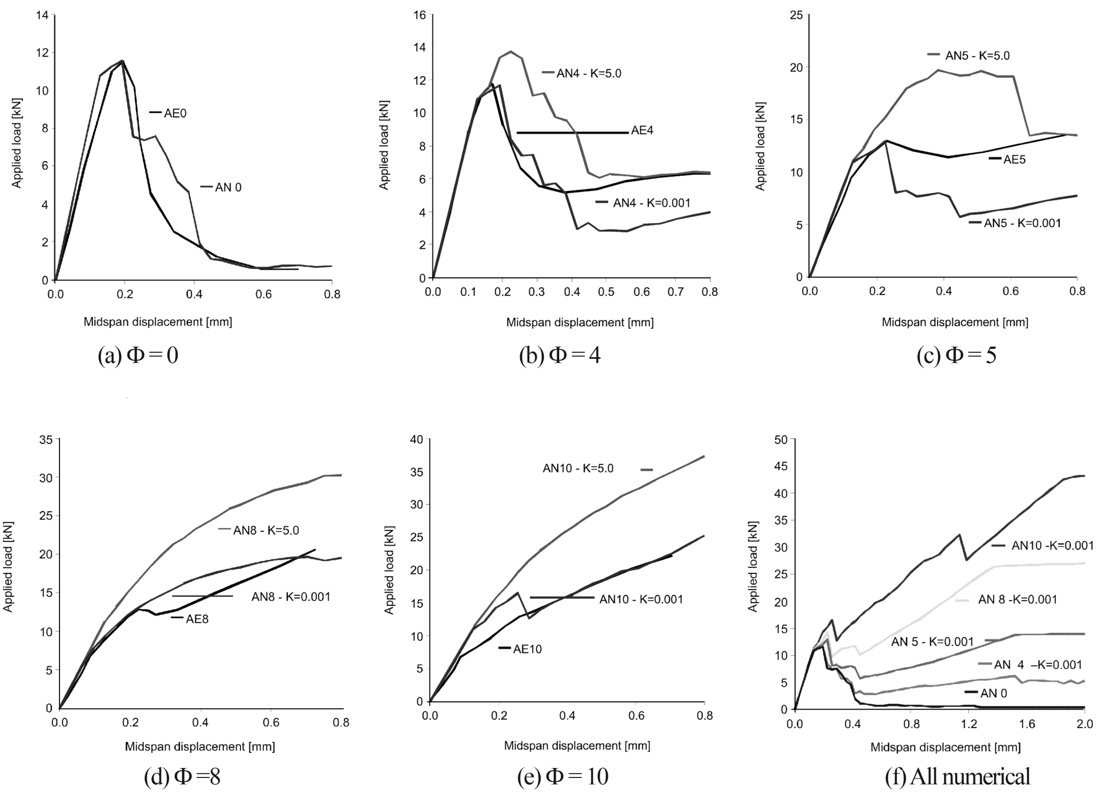

Fig. 10 Three point bending test – load versus displacement diagrams

towards the loading plate crossing the reinforcement bar. As the crack needs to transverse the particle boundary, a certain degree of tortuosity is found in the final crack patterns.

Table 2 shows the average maximum loads recorded both in the numerical and in the experimental tests. The axial stiffness of the interface is proportional to the rigid bar element lumped stiffness through a “K” multiplier. It can be verified that, given a previous calibration procedure in order to set the micro-properties through uniaxial compression and tensile tests, the reinforced particle model is capable of matching the maximum load on a different geometry (beam) and with different loading conditions (bending). Table 2 also indicates that a higher stiffness bond for the steel/concrete interface, $K = 5.0$ leads to an increase of the maximum load values.

Fig. 10 compares the numerical and experimental load displacements diagrams obtained for several reinforcement solutions. It is possible to verify that, for the case without reinforcement, the numerical solution agrees well with the experimental data.

Fig. 10 shows a good agreement between the experimental tests and the numerical test adopting a bond-slip relationship, numerically defined through a smaller axial interface stiffness, $K = 0.001$. It can also be seen that after the on-setting of cracking the numerical model with a higher stiffness bond, closer to a perfect bond model, gives a too stiff response. Note that in the simulations here presented the interfaces never reached their maximum axial strength, so the bond-slip relationship is still within the elastic range. When cracking occurs around the reinforcement, it is expected that the load transfer between the concrete particles and the reinforcement bars should be reduced and that higher slip occurs between the materials.

Fig. 10(f) clearly shows that the response of a reinforced concrete beam can be made more ductile by increasing the steel reinforcement ratio. It can be seen that the transition between brittle and plastic response occurs for a reinforcement ratio above $2\Phi5$ (as observed in the experiment).

The reinforcement particle assembly is shown to predict the maximum load for a given three point bending system, under a flexure loading condition. The model is also shown to match the expected crack pattern and crack growth. The response of the model with a higher stiffness, closer to a perfect bond, is shown to be more rigid than the real one after cracking. Even tough there are limitations in a 2D interface model, as the 3D effect of the crack versus loss of bond is complex, it can be seen that there are advantages in adopting a model which takes into account a bond-slip law when compared with a model that adopts a perfect bond. The bond-slip model with a lower stiffness allows a redistribution of forces around the particle assembly. The value of the stiffness adopted for the axial case should be also calibrated through pull-out tests if they were available for the experimental tests here analyzed, as it is shown that the stiffness of the interface influences the overall response.

Fig. 11 shows the axial stress distribution over the reinforcement bars for the numerical tests with 8.0 mm reinforcement. As shown, the model with a higher bond stiffness, $K = 5.0$, increases the extension in which the yield stress value is occurring. This effect leads to a higher stiffness when compared with the case where a lower bond-slip stiffness is adopted. Note that this phenomena occurs for all the reinforcement sizes that were tested.

At failure, the reinforcement bar axial stress has reached its yield limit and just a small portion of the particle structure, around 3 particles diameters in depth, just below the upper plate is still transferring contact forces to each side of the plate. Note that only in the AE10 numerical test the contact stress in this zone, closer to the upper plate, has reached a value (110 MPa) higher than the concrete maximum compression test (91.2 MPa), which can still be considered to be closer to the maximum value.

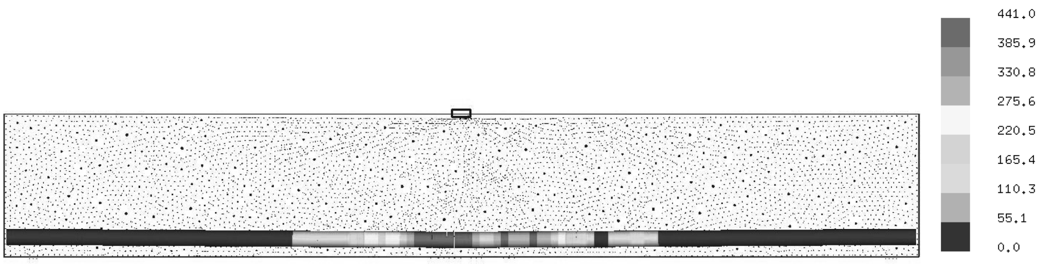

(a) Higher stiffness bond

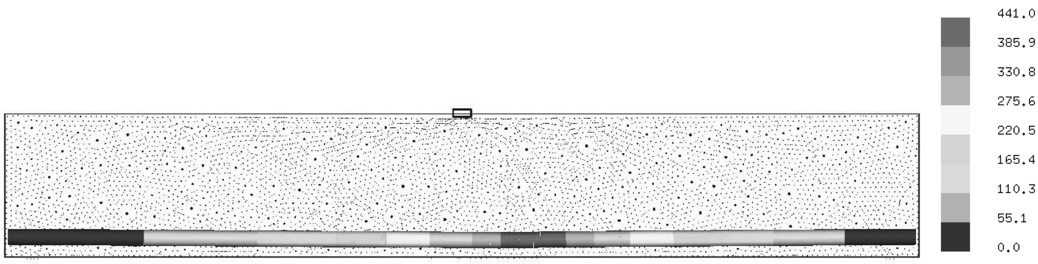

(b) Lower stiffness bond

Fig. 11 Three point bending test – reinforcement axial stress [MPa] – AE8 (2Φ8)

It would be possible to limit the maximum interparticle contact compression stress to 91.2 MPa in order to attempt to model concrete crushing in 2D, but in the tests present it was not relevant as this maximum value was not reached. For higher steel ratio's then the one here tested this phenomena would be more relevant and obviously it would be important to either adopt a 3D model that can accurately model concrete crushing or to adopt a maximum compression contact criteria in 2D.

3.2 Four point bending test

A four point bending geometry shown in Fig. 12 was also tested using the 2D enhanced reinforced particle model. The tested model was used in Bazant and Kazemi (1991) to study the size effect on diagonal shear failure of reinforced concrete without stirrups. The micro-concrete, made of aggregate with a maximum size of 4.8 mm, had an average compressive strength of 46.8 MPa measured on cylinders with 76 mm in diameter and 152 mm high. The longitudinal bars had a yielding point varying between 690 MPa to 890 MPa. All the tested geometries had a constant thickness of 38.1 mm.

The micro properties, best-fit macroscopic numerical values obtained from a calibration procedure based on compressions tests in 80 by 160 mm rectangular particle assemblies are given in Table 3, also given, are the macroscopic compressive strength, σ_c, Young's modulus, E, and Poisson's ratio, ν, obtained numerically. In the particle generation procedure an aggregate content of 568.5 kg/m^3 for a particle size between 4.8 and 2.0 mm was adopted. In order to fill the void space around the aggregate structure, a void elimination procedure, see Monteiro Azevedo and Lemos (2006), was

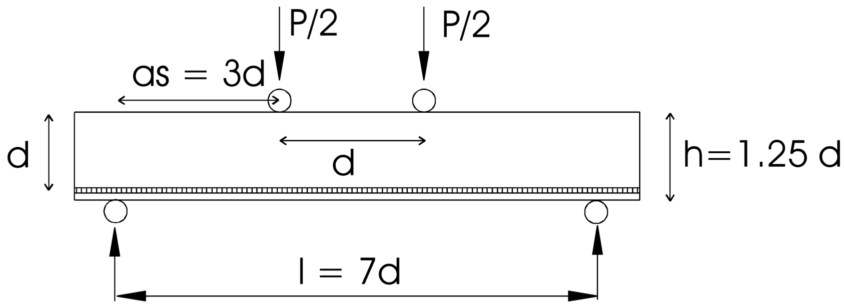

Fig. 12 Four point bending test geometry

Table 3 Elastic and strength properties for the particle model for the four point bending test

E_c [GPa]	ν_c	σ_t^c [MPa]	C^c [MPa]	μ^c [MPa]	G_{ft}^c [N/m]	G_{ct}^c [N/m]
28.0	0.25	2.8	13.0	0.2	10	500

(a) Micro-properties

E [GPa]	ν	σ_c [MPa]
35.1	0.21	47.6

(b) Macro-properties

carried out by inserting particles with a 2.0 mm diameter. Two different values for *d*, the distance from the compression face to the centre of the tensile reinforcement, were adopted: 40.64 mm and 81.28 mm. The reinforcement bars adopted for each size were, respectively, 25.8 mm^2 and 52.4 mm^2. In the numerical simulations, an intermediate size of *d* equal to 60.96 mm with a reinforcement area of 39.0 mm^2 was also considered.

In all cases, the reinforcement was modelled through rigid bars with a length of approximately 2.0 mm, adopting a linear elastic model followed by a yield plateau for a stress equal to 790 MPa. The reinforcement had a Young's Modulus of 200.0 GPa. As in the previous test, a linear elastic behaviour with a maximum axial interface strength given by CEB-FIP (1990) for confined concrete was adopted. In the tests performed this maximum axial force was never reached. The interface axial stiffness is also proportional to the rigid bar contact axial stiffness and the same values of the multiplying factor "K" referred in the bending test were adopted.

For each size, two different reinforced particle assemblies were tested. Fig. 13(a) shows one of the reinforced particle assemblies adopted for the size $d = 60.96$ mm. The smaller reinforced particle assemblies had on average 600 aggregate particles of a total of 4000 particles, whereas the larger particle assemblies had 2500 aggregate particles of a total of 15000 particles.

Fig. 13(b) shows the final crack pattern obtained. On all tested sizes and assemblies the following crack growth occurred. First, several tensile cracks appeared underneath the reinforcement in the zone of maximum bending moment (central part mid-span). Next, several tensile cracks appeared at the middle zone above the reinforcement. At one of such cracks, the one furthest away from the central part, a crack grew diagonally towards the loading plate above and towards the support underneath. In most of the tests, only one diagonal crack was identified, but sometimes a secondary diagonal crack developed opposite to the initial diagonal crack growing towards both supports. The diagonal cracks are formed by an array of *en echelon* splitting cracks.

Fig. 14(a) compares the average maximum load value obtained in the experiments and in the

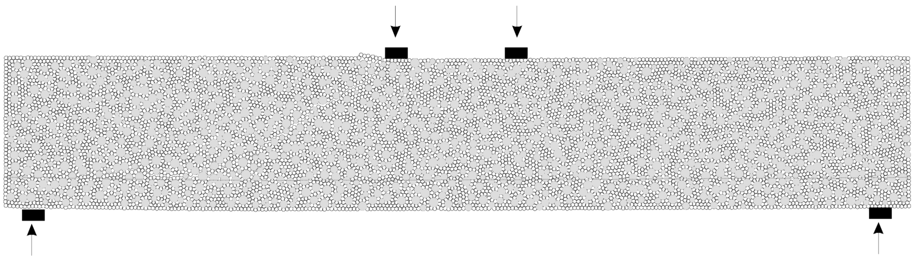

(a) Reinforced particle assembly

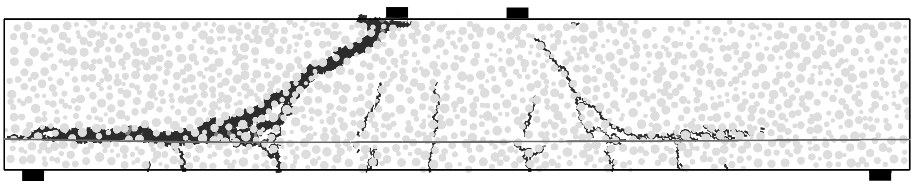

(b) Final crack pattern

Fig. 13 Four point bending test – d = 60.96 mm

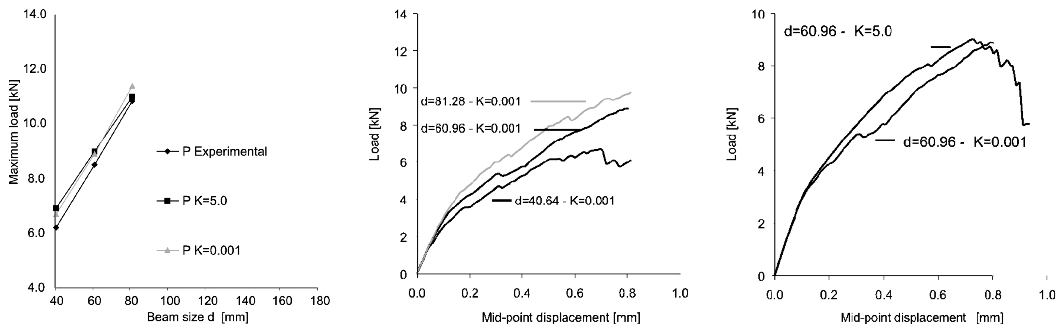

(a) Load versus size (Experimental and numerical)

(b) Load versus displacement – size (Numerical)

(c) Load versus displacement – bond type (Numerical)

Fig. 14 Four point bending test – experimental and numerical results

numerical simulations. It can be seen that the numerical response gives maximum loads closer to the experimental ones. It can also be seen that, in this experiment, the type of stiffness adopted on the bond-slip relationship does not influence significantly the maximum load. Fig. 14(b) shows the load displacement diagrams for the lower bond stiffness.

From Fig. 14(c), one can identify that a higher stiffness bond, closer to a perfect bond, increases the post-peak ductility. For this reason it is important to have a flexible interface model which allows bond slip in order to have a material response closer to the real one.

4. Conclusions

A rigid particle model that captures the fracture mechanisms by taking into consideration the concrete aggregate structure and the physical mechanisms related to the contact interaction is described. A rigid discrete bar model for the reinforcement and an interface model, which enables force transference between the particle assembly and the reinforcement, are proposed. The latter enhancements enable the application of the particle model to reinforced concrete structures.

It is shown that it is possible to calibrate the micro-properties of the particle model in order to obtain elastic, strength and fracture macro-responses similar to the ones observed in reinforced concrete structures under different loading conditions. The calibration procedure needs to be performed for traditional fracture tests prior to the application of the model to other structural systems. Assemblies of discrete particles connected through simple interaction laws are able to capture the global behaviour of reinforced concrete. Even if a simple trial-error calibration has been performed it is shown that a more complex behaviour under different geometry and loading condition can be predicted if the same particle generation procedures are adopted.

Under three point bending loading, the reinforcement model is shown to capture well the load displacement response, the peak load, the final crack pattern and the crack growth process for several reinforcement ratios. The model is also shown to predict the transition of the response from brittle to plastic as the reinforcement ratio is increased. When comparing a high stiffness bond-slip law, closer to a perfect bond, with a lower stiffness bond-slip law, the latter is able to model the reduction of stiffness which occurs when cracking first occurs by allowing a redistribution of forces.

Under four point loading conditions the reinforced particle model is shown to predict the expected crack evolution and localization. The numerical response leads to maximum loads closer to the maximum loads experimentally observed. For these tests the type of bond-slip stiffness value adopted for the concrete/steel interface does not have a significant effect on the overall response both in terms of the maximum load and crack process. This occurs because the crack only occurs closer to the reinforcement in the latter stages of the simulation. The numerical reinforced model proposed is able to predict the size effect on diagonal shear failure of beams without stirrups which is known to be a difficult problem to deal with other numerical models.

The reinforced concrete model presented can be used as an auxiliary tool by the experimentalist in order to enhance his understanding of the experiments and to study the influence of some of the mechanisms explicitly considered in the particle model. In large scale tests the model can be applied only in the zone of the model where nonlinearity is expected, adopting a finite element mesh on the remaining areas.

The explicit formulation here proposed for the reinforcement, modelled by rigid bars, can be readily extended to 3D, these elements with a cylindrical shape would interact through its surface with the spherical particles modelling concrete.

References

ASCE Committee on Concrete and Masonry Structures (1981), *Finite element analysis of reinforced concrete, Task Committee on Finite Element Analysis of Reinforced Concrete Structures of the Structural Division Committee on Concrete and Masonry Structures*, ASCE Special Publication.

Bazant, Z. (1986), "Mechanics of distributed cracking", *Appl. Mech. Rev., ASME*, **4**(5), 675-705.

Bazant, Z. and Kazemi, M.T. (1991), "Size effect on diagonal shear failure of beams without stirrups", *ACI-Struct. J.*, **88**, 268-276.

Berton, S. and Bolander, J.E. (2006), "Crack band model of fracture in irregular lattices", *Comput. Meth. Appl. Mech. Eng.*, **195**, 7172-7181.

Bolander, J.E. and Le, B. (1999), "Modeling crack development in reinforced concrete structures under service loading", *Constr. Build. Mater.*, **13**, 23-31.

Bosco, C., Carpinteri, A. and Debenardi, P. (1990), "Minimum reinforcement in high strength concrete", *J. Struct. Eng.*, **116**, 427-437.

Comité Euro International du Béton (1990), CEB-FIP Model Code 1990, First Draft, CEB, Paris.

Caballero, C., Lopez, C.M. and Carol, I. (2006), "3D meso-structural analyis of concrete specimens under uniaxial tension", *Comput. Meth. Appl. Mech. Eng.*, **195**, 7182-7195.

Chen, G. and Baker, G. (2003), "Influence of bond Slip on crack spacing in numerical modeling of reinforced concrete", *J. Struct. Eng.-ASCE*, **129**(11), 1514-1521.

Cundall, P. and Strack, O. (1979), "A discrete numerical model for granular assemblies", *Geotechnique*, **29**(1), 47-65.

Cusatis, P., Bazant, Z. and Cedolin, L. (2003), "Confinement-shear lattice model for concrete damage in tension and compression: I. Theory", *J. Eng. Mech.,* **129**(12), 1439-1448.

Hentz, S., Daudeville, L. and Donzé, V. (2004), "Identification and Validation of a discrete element model for concrete", *J. Eng. Mech.-ASCE*, **130**(6), 709-719.

Lilliu, J.G. and Van Mier, M. (2003), "3D lattice type fracture model for concrete", *Eng. Fract. Mech.,* **70**, 841-927.

Lorig, L. and Cundall, P. (1987), "Modeling of reinforced concrete using the distinct element method", SEM/RILEM International Conference on Fracture of Concrete and Rock (Eds. S. Sha and S. Swartz), Houston, 459-471.

Kawai, T. (1978), "New discrete models and their application to seismic response analysis of structures", *Nucl. Eng. Des.*, **48**, 207-229.

Meguro, K. and Hakuno, M. (1989), "Fracture analysis of concrete structures by the modified distinct element method", *Struct. Eng. Earthq. Eng.*, **6**(2), 283-294.

Monteiro Azevedo, N. (2003), "A rigid particle discrete element model for the fracture analysis of plain and reinforced concrete", PhD Thesis, Heriot-Watt University, Scotland.

Monteiro Azevedo, N. and Lemos, V. (2006), "Aggregate shape influence the fracture behaviour of concrete", *Struct. Eng. Mech.,* **24**(4), 411-427.

Morikawa, H., Sawamoto, Y. and Kobayashi, N. (1993), "Local fracture analysis of a reinforced concrete slab by the discrete element method", *Proceedings of the 2nd International Conference on Discrete Element Methods*, Cambridge, Massachusetts, IESL Publications, 275-286.

Ngo, D. and Scordelis, A. (1967), "Finite element analysis of reinforced concrete", *ACI J.*, **64**(44), 152-163.

Potyondy, D. and Cundall, P.A. (1996), "Modeling rock using bonded assemblies of circular particles", *Proceedings of the 2nd North American Rock Mechanics Symposium*, Montreal, June.

Potyondy, D.O. and Cundall, P.A. (2004), "A bonded-particle model for rock", *Int. J. Rock Mech. Min.,* **41**, 1329-1364.

Rokugo, K. (1989), "Testing method to determine tensile softening curve and fracture energy of concrete", *Fracture Toughness and Fracture Energy,* Balkema, 153-163.

Saito, S. and Hikosaka, H., (1999), "Numerical analyses of reinforced concrete structures using spring network models", *J. Materials Conc. Struct., Pavements, JSCE*, **627**(44), 289-303.

Schlangen, E. and Garboczi, E. (1996), "New method for simulating fracture using an elastically uniform random geometry lattice", *Int. J. Eng. Sci.*, **34**(10), 1131-1144.

Takada, S. and Hassani, N. (1997), "Modeling of reinforced concrete structures during earthquake", *Proceedings of the 4th International Conference on Civil Engineering*, Tehran.